A technique for mapping hourly global solar near infrared radiation from satellite data

Korntip Tohsing[1], Serm Janjai[1,*], Itsara Masiri[1], Manuel Nunez[2], Noppamas Pratummasoot[3] and Warangkana Thongrasmee[1]

[1] Solar Energy Research Laboratory, Department of Physics, Faculty of Science, Silpakorn University, Nakhon Pathom 73000, Thailand
[2] Geography and Environmental Studies Discipline, School of Land and Food, University of Tasmania, Hobart 7001, Australia
[3] Applied Physics Program, Faculty of Science and Technology, Valaya Alongkorn Rajabhat University under the Royal Patronage, Pathum Thani 13180, Thailand
***Corresponding author's email:** serm.janjai@gmail.com
Received: 12/12/2018, Accepted: 10/04/2019

Abstract

This paper presents a technique for mapping hourly global solar near infrared radiation (SNIR) from 0.695μm to 2.80 μm using MTSAT-1R satellite data. A simple radiative balance model is used to relate an atmospheric reflectance as seen by the satellite to an equivalent reflectance obtained from pyranometer measurements in the SNIR band. The tuned and calibrated atmospheric reflectance from satellite data is then used to estimate surface SNIR irradiance and the results are shown as SNIR maps. Statistics for monthly average of hourly SNIR irradiance are presented for Thailand using five years (2009-2013) of satellite data.

Keywords:

solar near infrared radiation; satellite data; mapping.

1. Introduction

Solar near infrared radiation (SNIR) at the earth surface, occupying mainly a spectral region between 0.695 μm to 2.80 μm, represents approximately half of the total solar spectrum [1-2]. As a result, SNIR contributes significantly the total radiant flux utilized by solar thermal energy systems in such activities as solar hot water systems and solar drying systems. It is also an important component of heat input of buildings, with consequences to their heating and cooling loads. Like broadband (0.3 μm -3.0 μm) solar radiation, SNIR is influenced by cloud and water vapor, which vary with location and time. Consequently, SNIR varies with location and time.

SNIR has not been investigated, to the same degree as other wavelength bands of the solar spectrum such as the UV or visible regions. A pioneering study by Gates et al. [3] measured the spectrum of SNIR at various altitudes up to 10,000 ft using an infrared spectrometer attached to a balloon. A later work by Bolsenga [4] investigated SNIR in Northern Greenland employing an Eppley pyranometer with Schott RG-8 filters. Some studies have attempted to partition SNIR as a fraction of broadband radiation for cloudless skies [5] and in South Americain more general conditions [6-7].

Information on SNIR is best obtained using a modelling approach as studies covering the tropical region are scarce compared to other parts of the solar spectrum, for example the ultraviolet and photosynthetically active radiation [8-9], and ground observations are few. In this study, we address the problem by developing an algorithm to estimate SNIR from satellite data, therefore providing a comprehensive regional coverage.

2. Methodology

2.1 Data acquisition and processing

Table 1 provides details of the data used. Surface irradiance in the SNIR (0.695 μm - 2.80 μm) was acquired using pyranometers (Eppley, model PSP) fitted with Schott glass filters RG-695 at four locations in Thailand: Chiang Mai (18.78°N; 98.98°E), Ubon Ratchathani (15.25°N; 104.87°E), Nakhon Pathom (13.82°N; 100.04°E) and Songkhla (7.20°N; 100.60°E) (Fig. 1). On a yearly basis the pyranometers are calibrated against a travelling standard which has been calibrated at the manufacturer and is traceable to the National Institute of Standard and Technology (NIST). Data is acquired every second by a data logger (Yokogawa, model DC100) and processed to hourly irradiation (J. m^{-2}. h^{-1}).

Fig. 1 Position of SNIR measurements and pictorial view of SNIR pyranometers. A, B, C and D indicate the northern, northeastern, central and the southern regions, respectively.

Table 1 Instrument details and data acquired in the study.

Source	Instrument	Duration	Acquisition Frequency	Area
Near infrared irradiance (0.695μm -2.80μm)	Eppley PSP pyranometer equipped with RG-695 filter	1/1/2009-31/12/2013	Every second integrated to hourly	4 locations: Chiang Mai (18.78°N; 98.98°E), Ubon Ratchathani (15.25°N; 104.87°E), Nakhon Pathom (13.82°N; 100.04°E) and Songkla (7.20°N; 100.60°E)
Reflectance of the earth atmospheric system (0.55 μm – 0.90 μm)	MTSAT-1R satellite	1/1/2009-31/12/2013	Hourly (8:30-16:30 local time)	5°N-21°N 96°E-106°E

Visible reflectance data was acquired on an hourly basis from the Japanese geostationary satellite MTSAT-1R. The raw signal in counts is converted into the earth-atmospheric reflectivity (ρ'_{EA}) using a conversion table provided by the satellite agency [10]. Each satellite image is then sectorized into a geographical area bounded by latitude: 5°N-21°N and longitude 96°-106°E, navigated using the local coastlines and transformed into the cylindrical projection linear in latitude and longitude. The final image has a pixel resolution of 3 km x 3 km.

Precipitable water data is needed for the satellite model and it was developed from relative humidity and air temperature data recorded at 85 meteorological stations throughout the country. Then the spline interpolation technique was applied to obtain precipitable water over the country [11-13].

A radiative transfer model from Tanre´ et al. [14] was used to derive a relationship between aerosol depletion and visibility and applied to visibility data recorded at 85 stations throughout the country. These estimations of depletion at discrete points were fitted with a minimum curve surface using the spline interpolation approach and therefore providing a monthly estimate of aerosol depletion [13]. The final step involved partitioning aerosol depletion into scattering and absorption which was done using the single scattering albedo from the AERONET data in the regions of East and Southeast Asia. Details of the expression are shown in Eqs. (4c) and (6) in the next section.

All data were acquired over a five-year period (1 January, 2009 – 31 December, 2013) and these were partitioned into two data sets. The period between 1 January, 2009 to 31 December, 2012 was used to build up a radiative model regression, essentially linking a satellite atmospheric reflectance to surface-derived reflectance as discussed in the next section. The resultant regression model was validated using an independent data set (1 January – 31 December, 2013).

After the validation, all data sets were turned into monthly averages for hourly values covering individual years. Therefore, a total of 60 individual months (5 years x 12 months) were processed. Each individual month was characterized by averages for 9 hours (8:00-9:00, 9:00-10:00, etc.). All model development, validation and statistics are performed with these hourly averages over the month. The reason being that this approach provides information on cloud-related diurnal changes, while at the same time removing random noise that may be caused by an individual cloud process at one specific hour.

2.2 Satellite model

Numerous studies have used satellite data to derive surface solar radiation using various approaches [15-22]. They range from simple regressions between satellite-derived reflectivity and pyranometer data [17] to one dimensional radiative transfer model which use look-up tables [23-24].

Much of the error in the satellite technique revolves around establishing a true cloud optical depth and reflectance from a single satellite view. One alternative used here is to relate, at a given location, the satellite-derived reflectivity to an atmosphere reflectivity needed to produce the required SNIR at the

surface. Fig. 2 shows the various steps involved. In Fig. 2a the satellite-derived earth-atmospheric reflectivity (ρ'_{EA}) is changed into an atmosphere reflectivity (ρ'_{A}) using a radiation balance model. These data are subsequently compared with an atmosphere reflectivity determined from the SNIR (ρ_{SNIR}) at the same location. In the second step (Fig. 2b) all the satellite data set is transformed into an atmosphere reflectivity which is then used to estimate SNIR.

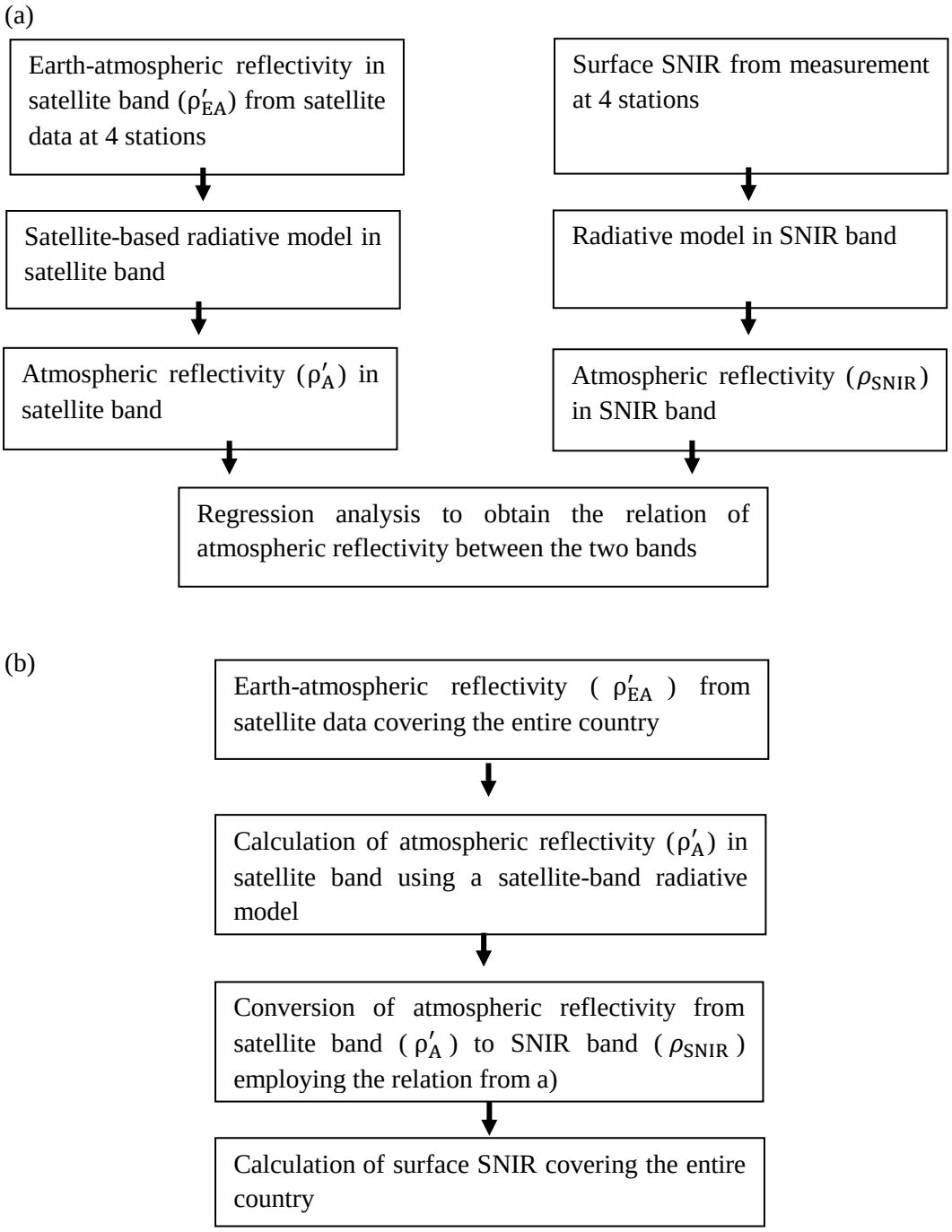

Fig. 2 Procedure for mapping SNIR from satellite data. (a) Development of the relation between atmosphere reflectivity in satellite band (ρ'_{A}) and SNIR band (ρ_{SNIR}). (b) The calculation process of surface SNIR covering the entire country.

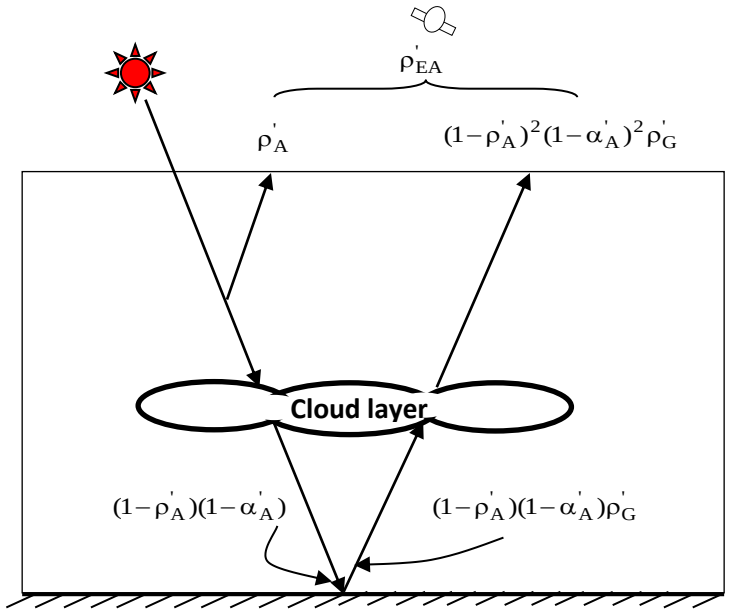

Fig. 3 Earth-atmosphere reflected solar radiation as detected by a satellite sensor. Greek symbols ρ and α represent scattering and absorption respectively while subscripts A and G refer to the atmosphere and ground, respectively. Primes refer to the satellite band. The first reflection represents radiation reflected from the atmosphere (ρ'_A), while the second represents radiation escaping to space after one reflection by the surface ($(1-\rho'_A)^2(1-\alpha'_A)^2\rho'_G$). All data is normalized to an incoming solar irradiance of 1.

Fig. 3 provides a schematic diagram of the satellite-derived reflectivity when the incoming solar irradiance is one. In this simple model, all scattering, and absorption terms are taken as equal in both the downwelling and upwelling directions. The radiation scheme adds all the outgoing radiation to space after reflection from the atmosphere only (ρ'_A), and one reflection by the surface $(1-\rho'_A)^2(1-\alpha'_A)^2\rho'_G$. Here ρ and α represent scattering and absorption respectively, while subscripts A and G refer to the atmosphere and ground respectively and primes refer to the satellite viewing band (0.55μm – 0.90 μm). The outgoing radiation to space (ρ'_{EA}) can be written as:

$$\rho'_{EA} = \rho'_A + (1-\rho'_A)^2(1-\alpha'_A)^2\rho'_G \quad (1)$$

Eq.(1) has one unknown, ρ'_A describing the reflection by the atmosphere, while the other terms are known: ρ'_{EA} is the satellite-derived reflectivity, ρ'_G is the surface reflectance and α'_A is the atmospheric absorption which includes water vapour, gasses, and aerosols. Therefore, Eq. (1) may be solved as a quadratic in ρ'_A:

$$\rho'_A = \frac{-B \pm \left(B^2 - 4AC\right)^{1/2}}{2A}$$
$$A = (1 - 2\alpha'_A + (\alpha'_A)^2)\rho'_G$$
$$B = (1 - 2\rho'_G + 4\alpha'_A\rho'_G - 2\rho'_G(\alpha'_A)^2) \quad (2)$$
$$C = (1 + (\alpha'_A)^2 - 2\alpha'_A)\rho'_G - \rho'_{EA}$$

The atmospheric absorption term may be expanded into its component terms:

$$\alpha'_A = \alpha'_{gas} + \alpha'_w + \alpha'_{aer}$$
$$\alpha'_i = 1 - \frac{\int_{0.55}^{0.90} I_\lambda \tau'_{i\lambda} d\lambda}{\int_{0.55}^{0.90} I_\lambda d\lambda} \quad (3)$$

where the subscripts "gas", "w" and "aer" refer to the absorption by atmospheric gases, water vapour and aerosol, respectively. Any of these terms may be expressed as a transmission (τ'_i) integrated over the satellite band and normalized by the extra-terrestrial irradiance in the satellite band (Eq. 3). Expressions for α'_{gas} and α'_W may be readily obtained from Leckner [25] as discussed in Iqbal [26] (Eqs. (4a) and (4b)), while the relationship for α'_{aer} is best described by the relationship from Janjai et al. [13] for the Thailand region (Eq. (4c)):

$$\tau'_{gas}(\lambda) = 1 - \alpha'_{gas}(\lambda) = \exp\left[(-1.41 k_{a\lambda} m)/(1 + 118.93 k_{a\lambda} m)\right] \quad (4a)$$

$$\tau'_W(\lambda) = 1 - \alpha'_W(\lambda) = \exp(-0.2385 k_{w\lambda} wm/(1 + 20.07 k_{w\lambda} wm) \quad (4b)$$

$$\alpha'_{aer} = [1 - (1.0358 - 0.3293(VIS)^{-0.66})^{m^{0.9}}](1 - \omega_0) \quad (4c)$$

where $k_{a\lambda}$ is an absorption coefficient for mixed gases in the atmosphere (dimensionless), $k_{w\lambda}$ is an absorption coefficient for precipitable water vapour (cm^{-1}), w is precipitable water vapour (cm), m is air mass (dimensionless), VIS is visibility in km and ω_0 is aerosol single scattering albedo. The term in the square brackets in Eq. (4c) represents the aerosol depletion for the Thailand region. It is multiplied by ω_0 which by definition is the ratio of the scattering to the total aerosol depletion [26]. The ω_0 term was obtained as a yearly average figure from the four Cimel sunphotometers located at each of the experimental sites which forms part of AERONET [27]. Precipitable water vapour for the Thailand region may be described in terms of a monthly average surface climatology [12]:

$$w = 0.893 \exp(0.1715 \times rh \times p_s / T) \quad (5)$$

where rh is relative humidity in decimal unit, p_s is saturated pressure in mbar and T is air temperature in K.

The scattering term $\rho_A^{'}$ is the sum of two terms $\rho_A^{'} = \rho_C^{'} + \rho_{aer}^{'}$ where $\rho_C^{'}$ represents the contribution from clouds and the atmosphere via Rayleigh scattering, and $\rho_{aer}^{'}$ is the scattering contribution by aerosol depletion, described as [13]:

$$\rho_{aer}^{'} = [1-(1.0358-0.3293(\mathrm{VIS})^{-0.66})^{m^{0.9}}]\omega_0 \tag{6}$$

where VIS is visibility in km.

The final term in the solution involves surface albedo. This term is high in the infrared spectrum but relatively low in the band covered by the satellite sensor (0.55 μm – 0.90 μm). We have used the IGBP spectral albedos as described by Moody et al. [28] for a mixture of evergreen broad forest and cropland with a 50% contribution from each. The authors provide spectral albedos at four wavelengths for a diffuse white sky. These were then linearly interpolated, and a weighted average albedo was obtained using the LIBRADTRAN [29] radiative transfer package:

$$\rho_G^{'} = \frac{\int_{0.55}^{0.90}\rho_G^{'}(\lambda)I_\lambda d\lambda}{\int_{0.55}^{0.90}I_\lambda d\lambda} \tag{7}$$

The global SNIR radiation as measured by a pyranometer sensor at the surface (τ_{SNIR}) may be expressed in a normalized form:

$$\tau_{SNIR} = \frac{G_{SNIR}}{G_{0SNIR}} = \frac{(1-\rho_{SNIR})(1-\alpha_{SNIR})}{1-\rho_{SNIR}\rho_{GSNIR}} \tag{8a}$$

$$\rho_{SNIR} = \frac{\tau_{SNIR}+\alpha_{SNIR}-1}{\tau_{SNIR}\rho_{GSNIR}+\alpha_{SNIR}-1} \tag{8b}$$

where G_{SNIR} is the measured SNIR, G_{0SNIR} is the extra-terrestrial SNIR and all other terms are as defined in Eq.(1) with the exception that the integration is performed over all the SNIR wavelengths (0.695μm to 2.80 μm). The transmission τ_{SNIR} is given as the product of a loss by scattering $(1-\rho_{SNIR})$ times loss by absorption $(1-\alpha_{SNIR})$ but enhanced by multiple scattering between the surface albedo (ρ_{GSNIR})and the atmosphere albedo (ρ_{SNIR}):$[1/(1-\rho_{SNIR}\rho_{GSNIR})]$.

We require a solution to ρ_{SNIR} as sensed by the pyranometer and it is given by Eq. (8b). All terms to the right of Eq. (8b) are known and may be estimated as in Eqs. (3) to (7) with a longer integration for SNIR wavelengths. The final step relates the satellite-determined monthly-averaged $\rho_A^{'}$ to the pyranometer estimate of monthly average ρ_{SNIR} at the four surface stations. Knowing the transformation, Eq. (8a) may be applied to estimate τ_{SNIR} at every pixel in the satellite image. Absolute irradiance is readily obtained by multiplying τ_{SNIR} by the extra-terrestrial irradiance (G_{0SNIR}) at a particular location.

3. Results

3.1 Model performance

Fig. 4 shows monthly average ρ'_A from the satellite at the four station locations vs estimates of ρ_{SNIR} for the period 1 January, 2009 to 31 December, 2012. A least square linear regression fit to the data gave the following statistics:

$$\rho_{SNIR} = 0.7142\,\rho'_A + 0.0863 \qquad (9)$$

$R^2 = 0.71$; SE = 0.061; n = 1146

with a highly significant R^2 at a level of confidence greater than 95%. SE is standard error and n is total number of data. Cloud reflection is largely independent of wavelength [26, 30] and this difference is likely to be a result of a decreasing Rayleigh scattering efficiency in the SNIR bands compared to the band occupied by the satellite sensor.

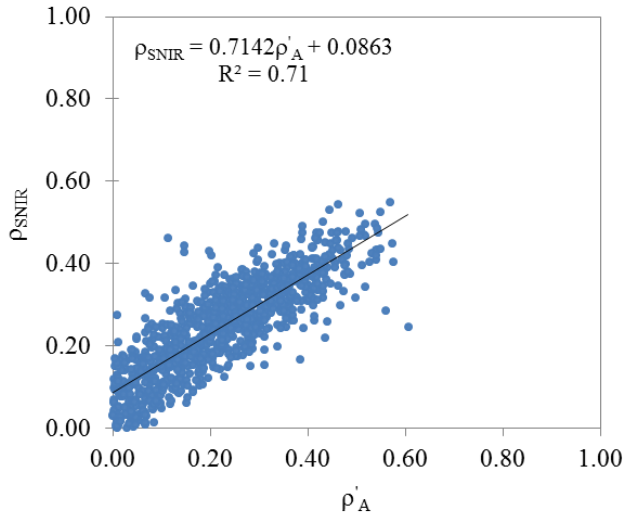

Fig. 4 Relationship between monthly average ρ'_A from the satellite estimates and ρ_{SNIR} obtained from the ground-based measurement at the four stations.

The normalized SNIR (τ_{SNIR}) may be obtained by applying the transformation in Eq. (9) to the normalized SNIR in Eq. (8a). Hourly average satellite-derived irradiances are plotted vs measured irradiances for the independent period of January – December, 2013 (Fig. 5). Irradiance for all four stations is used, involving a total of 432 data pairs (4 stations x 12 months x 1 year x 9 hours). The independent validation is satisfactory with a mean bias difference (MBD) of 3.7% which approaches instrumental errors of 2% and a root mean square difference (RMSD) of 16.0%.

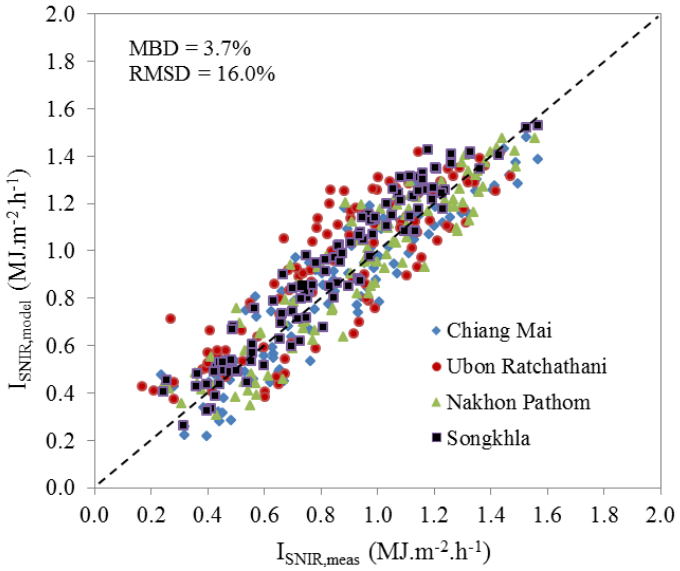

Fig. 5 Comparison between hourly average SNIR obtained from the measurement ($I_{SNIR,meas}$) and that calculated from the model ($I_{SNIR,model}$).

3.2 Statistics of monthly average hourly SNIR

Fig. 6 –8present hourly average maps for each month at representative times 9:30, 12:30 and 15:30 local time. Each hourly map is an average of 1825 images (365 days x 5 years) and is therefore a robust statistic. Examining the morning images (Fig. 6) there is a yearly signal with low values at the start and end of the year, and high values during mid-year. In addition, there are pronounced regional maxima in the eastern section of the country, with the highest readings (0.8 – 0.9 MJ.m^{-2}.h^{-1}) occurring in the dry months before the full onset of the Southwest monsoon, April, May and June. The pattern is likely to be a result of two factors. Firstly, the solar zenith angle in the early morning is lower in the eastern part of the country, which is also characterized by a less frequent cloud cover.

The noontime maps taken at 12:30 (Fig. 7) do not feature a distinct yearly signal and the irradiance appears to be more evenly distributed compared to the morning maps. There are, however indications of a weak maxima (1.3-1.4 MJ.m^{-2}.h^{-1}) occurring in the central part of the country, very likely due to cloud cover effects.

Generally lower irradiance is displayed in the late afternoon images estimated at 15:30 (Fig. 8). Cloud development is likely to reach maximum intensity at this time, and this process is likely to blur any regional differences. There is however an east-west gradient appearing in January to April, probably a result of lower solar zenith angles in the eastern section of the country at this time.

It is interesting to investigate the spatial distribution of yearly average daily SNIR. To accomplish this, monthly average hourly SNIR for each hour was summed over the day to obtain daily SNIR.

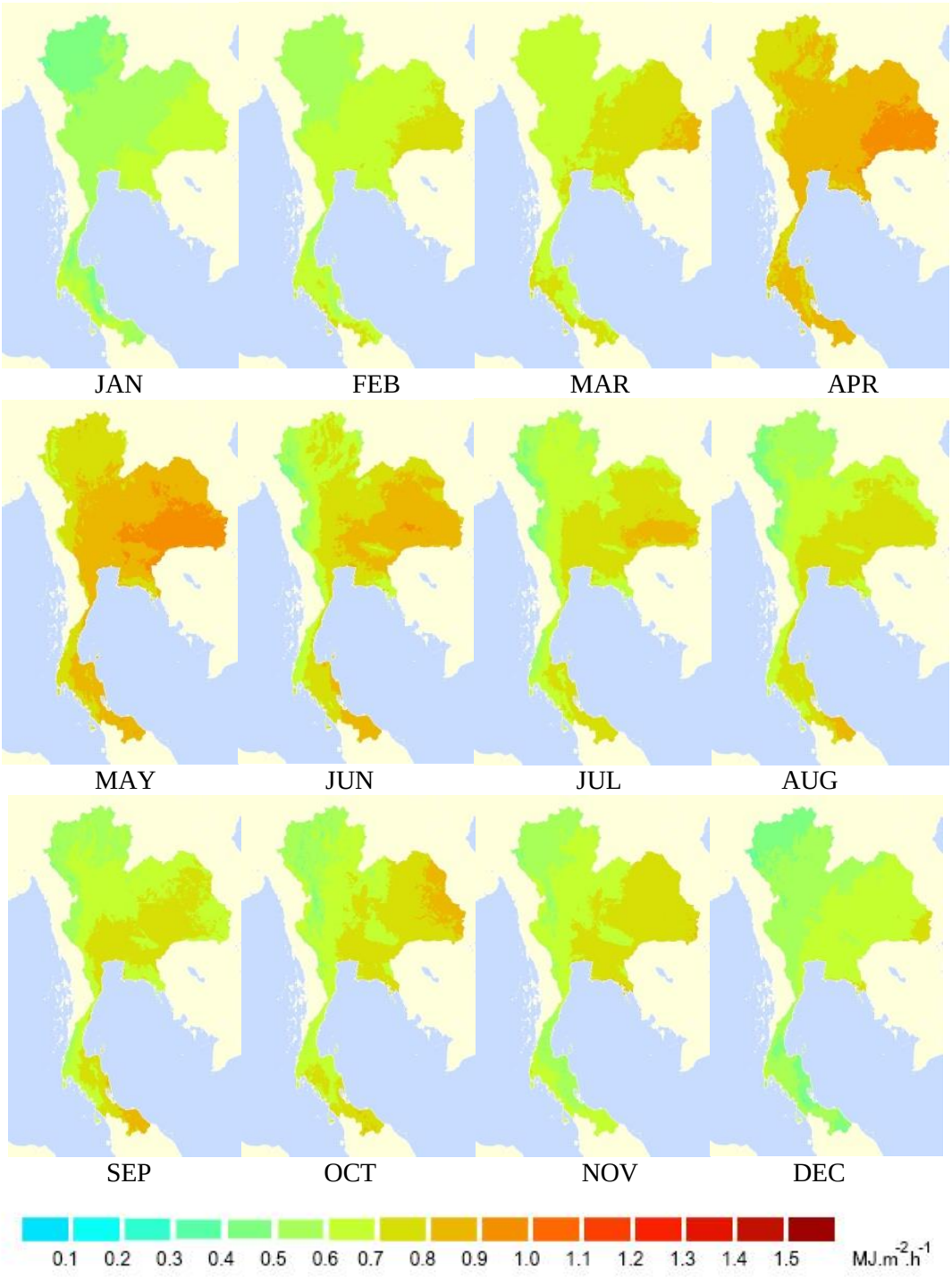

Fig. 6 The monthly average hourly SNIR maps for all months at 9:30 h.

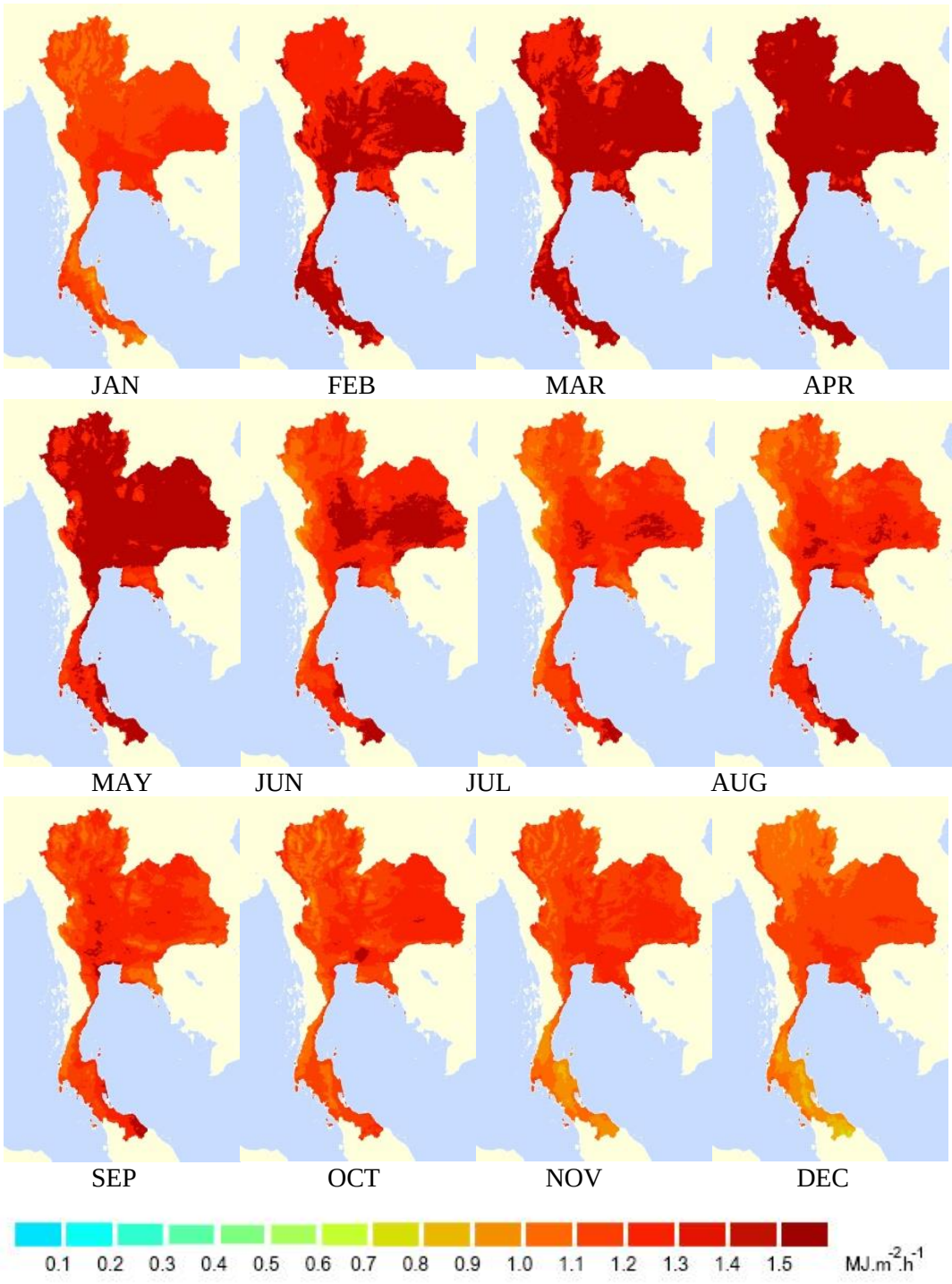

Fig. 7 The monthly average hourly SNIR maps for all months at 12:30 h.

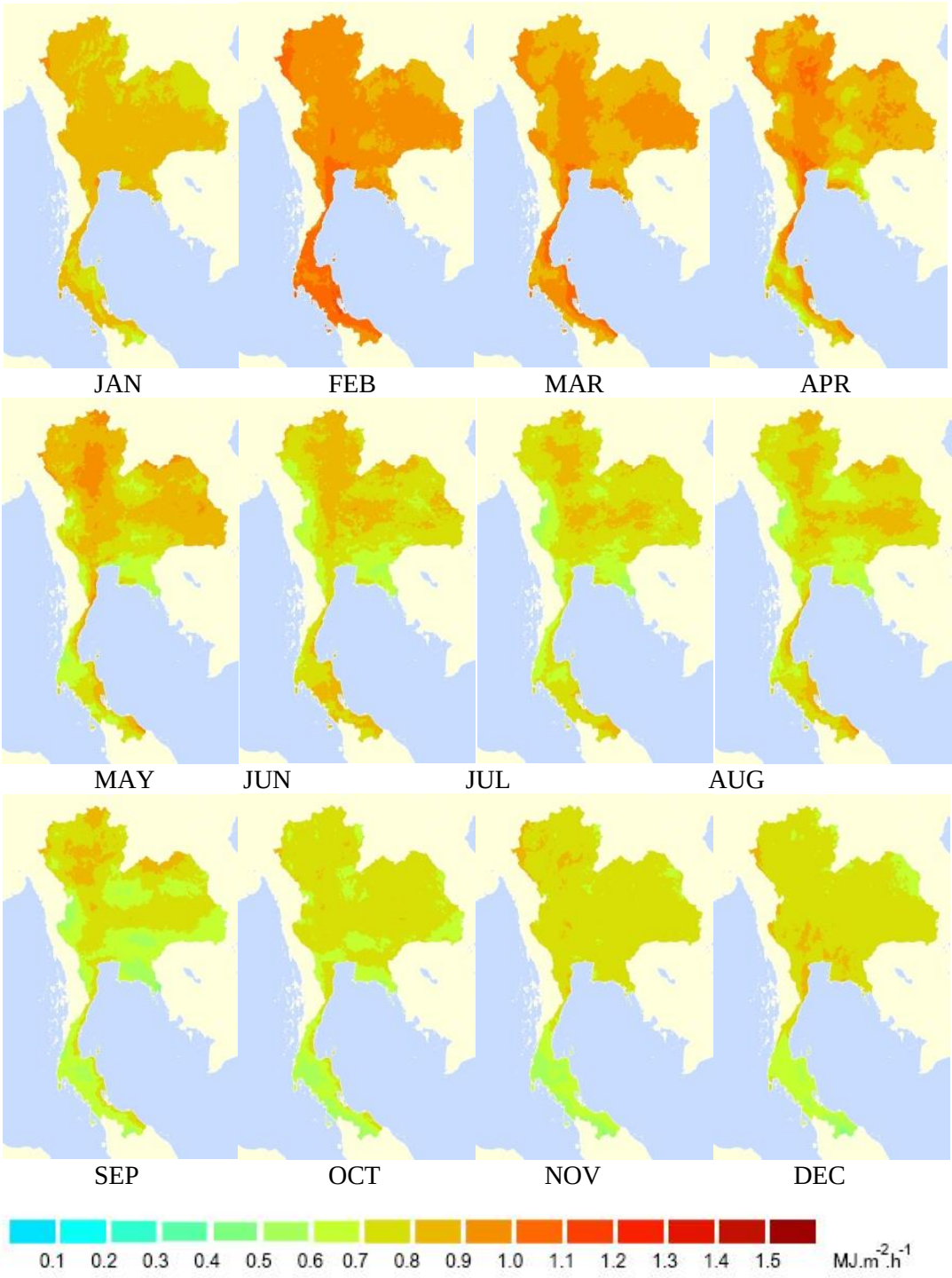

Fig. 8 The monthly average hourly SNIR maps for all months at 15:30 h.

4. Conclusions

The study has developed a method to estimate hourly global solar near infrared irradiance at the earth's surface in the Thailand region. The approach combines visible reflectance data from the MTSAT-1R satellite and solar near infrared irradiance measurements from four stations in Thailand. Using a simple radiation budget model, hourly atmospheric reflectance from the four stations are related to a satellite-derived atmospheric reflectance. Surface solar near infrared irradiance in the Thailand region may then be estimated using a simple radiation model which uses a corrected satellite-derived atmospheric reflectance.

Maps of monthly average hourly irradiance are presented at three different times of the day and for all 12 months. They show significant seasonal variability with maxima during mid-year and a tendency for irradiance to be largest in the central and northeastern regions of the country. On a diurnal basis the maxima occur at noon followed by the morning observation and with the lowest values in late afternoon, which is likely a result of cloud development and high solar zenith angle.

Acknowledgements

The authors would like to thank Silpakorn University Research and Development Institute for financially supporting this research work. We are also grateful to the Thailand Research Fund (TRF) for a partial support to the work under its International Research Network (IRN) program. Finally, we thank Thai Meteorological Department for support the measurements of solar near infrared radiation at its regional centers.

References

[1] Petty, G.W. (2004). A first course in atmospheric radiation. sundog publishing, Madison.

[2] Muneer, T. (2004). Solar radiation and daylight models. Elsevier Butterworth-Heinemann, Oxford, UK.

[3] Gates, D.M., Murcray, D.G., Shaw, C.C., & Hevbold, R.J. (1958). Near infrared measurements by balloon to an altitude of 10,000 feet. *Journal of the Optical Society of America, 43,* 1010-1016.

[4] Bolsenga, S.J. (1976). Near infrared radiation in Northern Green land. *Journal of Applied Meteorology and Climatology, 6,* 449 – 451.

[5] Weiss, A., & Norman, J.M. (1985). Partitioning solar radiation into direct and diffuse, visible and near infrared components. *Agricultural and Forest Meteorology, 34,* 205-213.

[6] Escobedo, J.F., Gomes, E.N., Oliveire, A.P., & Soares, J. (2009). Modeling hourly and daily of UV, PAR and NIR to global solar radiation under variation sky conditions at Botucatu, Brazil. *Applied Energy, 86,* 299 – 309.

[7] Rossi, T.J., Escobedo, J.F., Dos Santos, C.M., Rossi, L.R., Da Silva, M.B.P., & Dal Pai, Enzo. (2018). Global diffuse and direct solar radiation of the infrared spectrum in Botucatu/SP/Brazil. *Renewable and Sustainable Energy Reviews, 82,* 448-459.

[8] Janjai, S., Buntung, S., Wattan, R., & Masiri, I. (2010). Mapping solar ultraviolet radiation from satellite data in a tropical environment. *Remote Sensing of Environment, 114,* 682-691.

[9] Choosri, P., Janjai, S., Nunez, M., Buntoung, S., & Charuchittipan, D. (2017). Mapping diffuse photosynthetically active radiation from satellite data in Thailand. *Advances in Space Research, 60,* 2345-2354.

[10] JMA. (2009). Conversion table of satellite data. Japanese Meteorological Agency, Tokyo, Japan.

[11] Cole, R.J. (1976). Direct solar radiation data as input into mathematical models describing the thermal performance of buildings – II. Development of relationships. *Building and Environment, 11,* 181-186.

[12] Janjai, J., Laksanaboonsong, J., Nunez, M., & Thongsathiya, A. (2005). Development of a method for generating operational solar radiation maps from satellite data for a tropical environment. *Solar Energy, 78,* 739-751.

[13] Janjai, S., Pankaew, P., & Laksanaboonsong, J. (2009). A model for calculating hourly global solar radiation from satellite data in the tropics. *Applied Energy, 86,* 1450 – 1457.

[14] Tanre´, D., Deroo, C., Duhaut, P., Herman, N., Morcrette, J.J., & Deschamps, P.Y. (1986). Simulation of the satellite signal in the solar spectrum. Techical Report, Laboratorire d´ Optique Atmospherique, Université des Science et Technique de Lille, 59655 Villeneuve d´ Ascq Cedex, France.

[15] Exell, RHB. (1984). Mapping solar radiation by meteorological satellite. *Renewable* and Sustainable *Energy Reviews,* 6, 27 – 39.

[16] Schillings, C., Mannstein, H., & Meyer, R. (2004). Operational method for deriving high resolution direct normal irradiance from satellite data. *Solar Energy, 76,* 475 – 484.

[17] Tarpley, J.D. (1979). Estimating incident solar radiation at the surface from geostationary satellite data. *Journal of Applied Meteorology and Climatology, 18,* 1172-1181.

[18] Gautier, C., Diak, G., & Masse, S. (1980). A simple physical model to estimate incident solar radiation at the earth surface from GOES satellite data. *Journal of Applied Meteorology and Climatology, 36,* 1005 – 1012.

[19] Nunez, M. (1993). The development of a satellite-based insulation model for the tropical western Pacific Ocean. *International Journal of Climatology, 13,* 607 – 627.

[20] Polo, J., Zarzaleja, L.F., & Ramírez, L. (2008). Solar radiation derived from satellite images. in: V. Badescu (Ed.), Modelling solar radiation at the earth's surface, Springer, Berlin, 449 – 461.

[21] Martins, F.R., Pereira, E.B., & Abreu, SL. (2007). Satellite-derived solar resource maps for Brazil under SWERA project. *Solar Energy, 81,* 517 – 528.

[22] Vonder, HT., Raschke, E., Bandeen, W., & Pasternak, M. (1973). Measurements of solar energy reflected by the earth and atmosphere from meteorological satellite. *Solar Energy, 14,* 175 – 184.

[23] Pinker, R.T., & Laszlo, I. (1992). Modeling surface solar irradiance for satellite applications on a global scale. *Journal of Applied Meteorology and Climatology, 31,* 194-211.

[24] Masiri, I., Nunez, M., & Weller, E. (2008). A 10-year climatology of solar radiation for the Great Barrier reef; implications for recent mass coral bleaching events. *International Journal of Remote Sensing, 29,* 4443-4462.

[25] Leckner, B. (1978), The spectral distribution of solar radiation at the earth's surface-elements of a model. *Solar Energy, 20,* 143-150.

[26] Iqbal, M. (1983). An Introduction to Solar Radiation, Academic Press, New York.

[27] Holben, B.N., Eck, T.F., Slutsker, I., Tanre´, D., Buis, J.P., Setzer, A., Vermote, E., Reagan, J.A., Kaufman, Y.J., Nakajima, T., Lavenu, F., Jankowiak, I., & Smirnov, A. (1998). AERONET- A Federated Instrument Network and data archeive for aerosol characterization. Remote Sensing of Environment 60, 1-16.

[28] Moody, E.G., King, M.D., Schaaf, C.B., Hall, C.B., & Platnick, S. (2007). Northern Hemisphere five-year average (2000-2004) spectral albedos of surfaces in the presence of snow: statistic computed from Terra MODIS land products. *Remote Sensing* of *Environment, 111,* 337 – 345.

[29] Mayer, B., & Kylling, A. (2005). Technical note: The libRadtran software package for radiative transfer calculations – description and examples use. Atmospheric Chemistry and Physics 5, 1855 – 1877.

[30] Stephens, G.L. (1994). Remote sensing of the lower atmosphere: an introduction. Oxford University Press Inc., Oxford.